DTU Library

Thermal tunability of photonic bandgaps in liquid crystal infiltrated microstructured polymer optical fibers

Yuan, Scott Wu; Wei, Lei; Alkeskjold, Thomas Tanggaard; Bjarklev, Anders Overgaard; Bang, Ole

Link back to DTU Orbit

Thermal tunability of photonic bandgaps in liquid crystal infiltrated microstructured polymer optical fibers

Wu Yuan,[1,*] Lei Wei,[1] Thomas Tanggaard Alkeskjold,[2]
Anders Bjarklev,[1] and Ole Bang[1]

*[1]DTU Fotonik, Dept. of Photonics Engineering, Technical University of Denmark,
DK-2800 Kgs. Lyngby, Denmark*
[2] NKT Photonics A/S, Blokken 84, DK-3460 Birkerød, Denmark
Phone: (+ 45) 4525 3979, Fax: (+ 45) 4593 6581
* wyuan@fotonik.dtu.dk,

Abstract: We demonstrate the photonic bandgap effect and the thermal tunability of bandgaps in microstructured polymer optical fibers infiltrated with liquid crystal. Two liquid crystals with opposite sign of the temperature gradient of the ordinary refractive index (E7 and MDA-00-1444) are used to demonstrate that both signs of the thermal tunability of the bandgaps are possible. The useful bandgaps are ultimately bounded to the visible range by the transparency window of the polymer.

OCIS codes: (060.2310) Fiber optics; (230.3990) Microstructure devices; (230.3720) Liquid-crystal devices.

References and links

1. R. T. Bise, R. S. Windeler, K. S. Kranz, C. Kerbage, B. J. Eggleton, and D. J. Trevor, "Tunable photonic band-gap fibre," in *Optical Fiber Communication Conference,* Vol. 70 of OSA Trends in Optics and Photonics Series (Optical Society of America, 2002), paper ThK3.
2. C. Kerbage, and B. J. Eggleton, "Numerical analysis and experimental design of tunable birefringence in microstructured optical fiber," Opt. Express **10**(5), 246–255 (2002).
3. T. T. Larsen, A. Bjarklev, D. S. Hermann, and J. Broeng, "Optical devices based on liquid crystal photonic bandgap fibres," Opt. Express **11**(20), 2589–2596 (2003).
4. T. T. Alkeskjold, J. Lægsgaard, A. Bjarklev, D. Hermann, A. Anawati, J. Broeng, J. Li, and S. T. Wu, "All-optical modulation in dye-doped nematic liquid crystal photonic bandgap fibers," Opt. Express **12**(24), 5857–5871 (2004).
5. F. Du, Y. Q. Lu, and S.-T. Wu, "Electrically tunable liquid-crystal photonic crystal fiber," Appl. Phys. Lett. **85**(12), 2181–2183 (2004).
6. M. W. Haakestad, T. T. Alkeskjold, M. D. Nielsen, L. Scolari, J. Riishede, H. E. Engan, and A. Bjarklev, "Electrically tunable photonic bandgap guidance in a liquid crystal filled photonic crystal fiber," IEEE Photon. Technol. Lett. **17**(4), 819–821 (2005).
7. T. R. Wolinski, K. Szaniawska, S. Ertman, P. Lesiak, A. W. Domanski, R. Dabrowski, E. Nowinowski-Kruszelnicki, and J. Wojcik, "Influence of temperature and electrical fields on propagation properties of photonic liquid-crystal fibres," Meas. Sci. Technol. **17**(5), 985–991 (2006).
8. D. C. Zografopoulos, E. E. Kriezis, and T. D. Tsiboukis, "Tunable Highly Birefringent Bandgap-Guiding Liquid-Crystal Microstructured Fibers," J. Lightwave Technol. **24**(9), 3427–3432 (2006).
9. T. T. Alkeskjold, J. Laegsgaard, A. Bjarklev, D. S. Hermann, J. Broeng, J. Li, S. Gauza, and S. T. Wu, "Highly tunable large-core single-mode liquid-crystal photonic bandgap fiber," Appl. Opt. **45**(10), 2261–2264 (2006).
10. L. Scolari, T. T. Alkeskjold, and A. Bjarklev, "Tunable Gaussian filter based on tapered liquid crystal photonic bandgap fibre," Electron. Lett. **42**(22), 1270–1271 (2006).
11. J. Lægsgaard, "Gap formation and guided modes in photonic bandgap fibres with high-index rods," J. Opt. A, Pure Appl. Opt. **6**(8), 798–804 (2004).
12. M. C. J. Large, L. Poladian, G. Barton, and M. Eijkelenborg, *Microstructured polymer optical fibres*, (Springer, 2008).
13. M. A. van Eijkelenborg, M. C. J. Large, A. Argyros, J. Zagari, S. Manos, N. A. Issa, I. Bassett, S. Fleming, R. C. McPhedran, C. M. de Sterke, and N. A. P. Nicorovici, "Microstructured polymer optical fibre," Opt. Express **9**(7), 319–327 (2001).

14. K. M. Kiang, K. Frampton, T. M. Monro, R. Moore, J. Tucknott, D. W. Hewak, D. J. Richardson, and H. N. Rutt, "Extruded singlemode non-silica glass holey optical fibres," Electron. Lett. **38**(12), 546–547 (2002).
15. G. Emiliyanov, J. B. Jensen, O. Bang, P. E. Hoiby, L. H. Pedersen, E. M. Kjaer, and L. Lindvold, "Localized biosensing with Topas microstructured polymer optical fiber," Opt. Lett. **32**(5), 460–462 (2007).
16. G. Emiliyanov, J. B. Jensen, O. Bang, P. E. Hoiby, L. H. Pedersen, E. M. Kjaer, and L. Lindvold, "Localized biosensing with Topas microstructured polymer optical fiber: Erratum," Opt. Lett. **32**(9), 1059 (2007).
17. K. Nielsen, H. K. Rasmussen, A. J. L. Adam, P. C. M. Planken, O. Bang, and P. U. Jepsen, "Bendable, low-loss Topas fibers for the terahertz frequency range," Opt. Express **17**(10), 8592–8601 (2009).
18. A. Dupuis, N. Guo, Y. Gao, N. Godbout, S. Lacroix, C. Dubois, and M. Skorobogatiy, "Prospective for biodegradable microstructured optical fibers," Opt. Lett. **32**(2), 109–111 (2007).
19. M. A. van Eijkelenborg, A. Argyros, A. Bachmann, G. Barton, M. C. J. Large, G. Henry, N. A. Issa, K. F. Klein, H. Poisel, W. Pok, L. Poladian, S. Manos, and J. Zagari, "Bandwidth and loss measurements of graded-index microstructured polymer optical fibre," Electron. Lett. **40**(10), 592–593 (2004).
20. R. Lwin, G. Barton, L. Harvey, J. Harvey, D. Hirst, S. Manos, M. C. J. Large, L. Poladian, A. Bachmann, H. Poisel, and K.-F. Klein, "Beyond the bandwidth-length product: Graded index microstructured polymer optical fiber," Appl. Phys. Lett. **91**(19), 191119 (2007).
21. A. Argyros, M. A. van Eijkelenborg, M. C. Large, and I. M. Bassett, "Hollow-core microstructured polymer optical fiber," Opt. Lett. **31**(2), 172–174 (2006).
22. F. M. Cox, A. Argyros, and M. C. J. Large, "Liquid-filled hollow core microstructured polymer optical fiber," Opt. Express **14**(9), 4135–4140 (2006).
23. M. H. Frosz, and. K. Nielsen, P. Hlubina, A. Stefani, O. Bang, "Dispersion-engineered and highly nonlinear microstructured polymer optical fibres," Proc. SPIE **7357**, 735705 (2009).
24. J. Jensen, P. Hoiby, G. Emiliyanov, O. Bang, L. Pedersen, and A. Bjarklev, "Selective detection of antibodies in microstructured polymer optical fibers," Opt. Express **13**(15), 5883–5889 (2005).
25. B. T. Kuhlmey, R. C. McPhedran, and C. Martijn de Sterke, "Modal cutoff in microstructured optical fibers," Opt. Lett. **27**(19), 1684–1686 (2002).
26. N. Litchinitser, S. Dunn, P. Steinvurzel, B. Eggleton, T. White, R. McPhedran, and C. de Sterke, "Application of an ARROW model for designing tunable photonic devices," Opt. Express **12**(8), 1540–1550 (2004).
27. S. G. Johnson, and J. D. Joannopoulos, "Block-iterative frequency-domain methods for Maxwell's equations in a planewave basis," Opt. Express **8**(3), 173–190 (2001).
28. J. Li, S. Gauzia, and S.-T. Wu, "High temperature-gradient refractive index liquid crystals," Opt. Express **12**(9), 2002–2010 (2004).

1. Introduction

It has previously been demonstrated that an initial index guiding silica photonic crystal fiber (PCF) can be converted to a highly tunable bandgap-guiding PCF by infiltrating the air holes with a suitable high-index material, such as a high-index fluid [1,2], or a Liquid Crystal (LC) [3–11]. It has also been shown that this allows for both thermal [3,7,9,10], electrical [5–8] and all-optical tuning [4], and makes it possible to achieve different functionalities, such as threshold switching [6], tunable birefringence controller [8], and tunable filter [10]. Compared with other materials, the attractive properties of LCs, i.e., the high birefringence, high electro-optic and thermo-optic effects, makes them the most suitable candidates for designing tunable all-in-fiber devices based on photonic bandgap effects.

Although most work in microstructured fibers has been reported in silica, other materials, such as polymers and soft glasses, are also increasingly explored [12–14]. Since the first fabrication of microstructured Polymer Optical Fibers (mPOFs) in Polymethyl methacrylate (PMMA, n=1.49 @589.3nm, 20°C) by Eijkelenborg *et al.* [13], mPOFs have been made using a variety of polymers, such as Topas (cyclic olefin copolymer) [15–17] and biodegradable polymers [18]. The standard single-mode mPOF has a triangular hole structure with a single hole size, but much more complicated hole structures can be made, such as the one used to make for example graded-index mPOFs [19,20]. Argyros et al. fabricated the first hollow-core bandgap mPOF with PMMA [21] and Cox el al. demonstrated that the bandgap effect can also be found in liquid-filled hollow-core mPOFs [22].

Compared with their silica counterparts, it is easier to fabricate exotic mPOFs by extrusion or drilling at low temperature, the nonlinearity is potentially stronger [23], the range of available polymers that may be drawn is more diverse [12] and the biocompatibility of polymers is often better [15,16,24]. This makes it potentially easier to tailor the functionalities of mPOF based fiber-optic devices and sensors [12,13]. Especially, PMMA mPOFs have

higher refractive index and possibly much more temperature tunability with orders of magnitude higher thermo-optic coefficient ($-1.1 \times 10^{-4}/°C$) than that of silica ($9.2 \times 10^{-6}/°C$) [12]. At the same time, the air holes in mPOFs may also be infiltrated with LC to create tunable polymer bandgap fibers.

Here, we infiltrate a PMMA index-guiding mPOF with LC and present for the first time, to the best of our knowledge, the LC induced bandgap effect in mPOF. Opposite signs of the thermal tunability of the bandgaps are further demonstrated by infiltrating identical mPOFs with two kinds of LCs, E7 and MDA-00-1444 (Merck, Germany), which have opposite temperature gradient of the ordinary refractive index (n_o).

2. mPOFs

The PMMA mPOF used in our experiment is fabricated with low tension in order to decrease the birefringence along the fiber axis. The resulting mPOF has a diameter of 140μm and a solid core surrounded by three rings of air holes arranged in a triangular lattice, as shown in the inset of Fig. 1. The air hole diameter (d) and inter-hole pitch (Λ) are 3.7±0.2μm and 7.8 ± 0.2μm, respectively. The mPOF is effectively single mode with a hole diameter to pitch ratio $d/\Lambda \approx 0.47$, which is close to the theoretical limit of 0.45 for endlessly single-mode behavior [25].
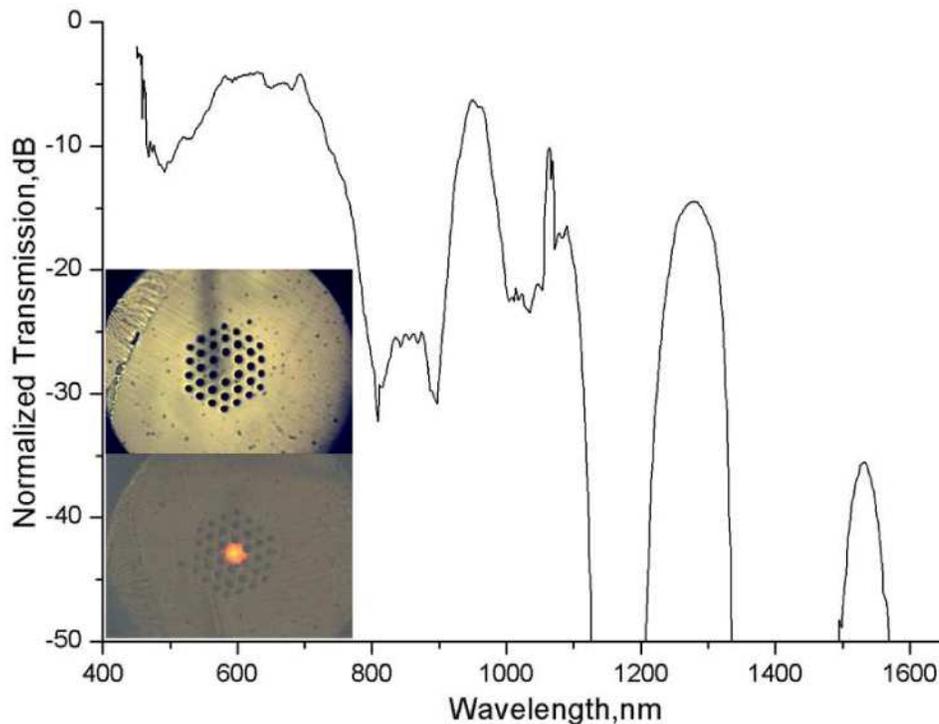

Fig. 1. Normalized transmission spectrum of a 60cm long PMMA mPOF. The insets show a microscope image of the fiber end facet before and after the fiber is pumped with a supercontinuum broadband light source.

The transmission spectrum of the mPOF is visualized with a microscope. A 60cm long mPOF is butt-coupled to a conventional single-mode fiber (SMF) and pumped with broadband light from a supercontinuum source (SuperK from NKT Photonics A/S, Denmark). The near field image of the fiber end facet before and after the broadband supercontinuum light is coupled is shown in the insets of Fig. 1. It is clear to see that the colour of the guided light is red. The normalized transmission spectrum of the mPOF is recorded by an optical

spectrum analyzer (OSA, Ando AQ6317B) with 1nm resolution and shown in Fig. 1. As we can see from Fig. 1, the material loss is huge in the near infrared range [12], creating gaps in the transmission spectrum, where effectively no light is transmitted. Low-loss bands, such as the one observed at 1200-1330mnm, could be mistaken for a bandgap if one is not careful. In order to avoid this complication and have a reasonably low loss, we therefore use the transparency domain of PMMA in the wavelength range below 850nm to study the bandgap effects in our following experiments.

Since mPOFs are more temperature sensitive than silica and cannot endure as high temperature as silica, we have also investigated the thermal stability of our mPOF to determine a suitable temperature range for our experiments. Checking a range of temperatures for up to 10 minutes there is no observable temperature dependence of the transmission at ambient temperatures below 60°C.

3. LCs and alignment of LCs in mPOFs

Positive dielectric anisotropy LCs E7 (n_o=1.52, n_e=1.74 @589.3nm, 20°C) and MDA-00-1444 (n_o=1.50, n_e=1.68 @589.3nm, 20°C) are used in this experiment. E7 has a positive temperature gradient of the ordinary refractive index, i.e., dn_o/dT=3.4×10^{-4}/°C at 40°C and 656nm [9], and its clearing temperature is 58°C. In contrast, MDA-00-1444 can provide a negative dn_o/dT, i.e. dn_o/dT=−2.2×10^{-4}/°C at 40°C and 656nm [10], and has a higher clearing temperature of 98.5°C.
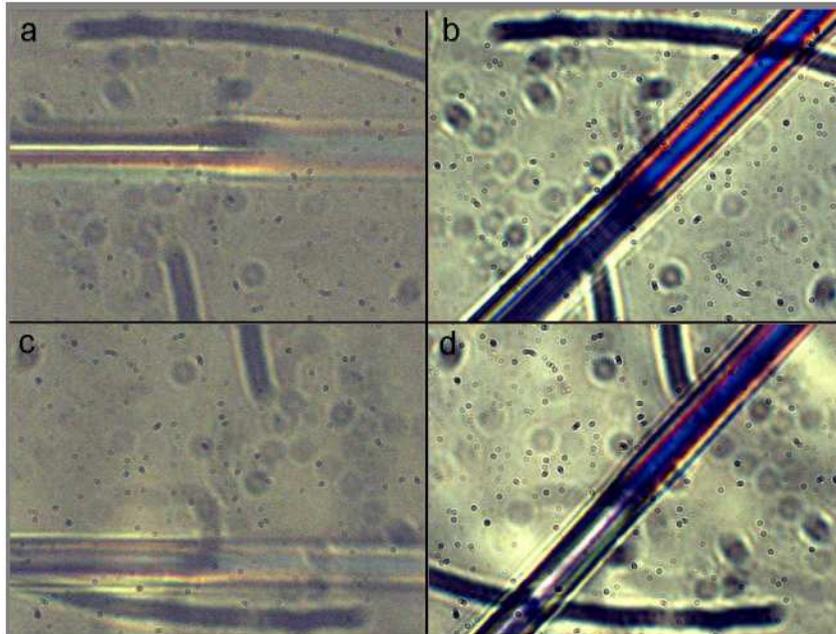

Fig. 2. Polarized microscope images of LC filled PMMA capillaries showing the interfaces between the filled and unfilled sections inside the capillary with orientation of 0° and 45°, respectively. (a-b) E7 infiltrated capillary, (c-d) MDA-00-1444 infiltrated capillary. The blue and colorful parts in (b) and (d) are the LC filled sections of the capillaries. All images are recorded by the microscope with two crossed polarizers.

As shown in Fig. 2, the polarized microscopy observations of a single PMMA capillary with an inner diameter of 5 um indicate that both E7 and MDA-00-1444 are homogeneously planar aligned, i.e., with the LC director aligned along the fiber axis. This is similar to the cases of E7 and MDA-00-1444 infiltrated into silica capillaries [4,6,10]. This alignment indicates that the ordinary indices (n_o) of E7 and MDA-00-1444 will predominantly

determine the spectral features of the LC infiltrated fibers. Furthermore, Fig. 2 also reveals that the PMMA capillaries are birefringent since the cladding parts of the tubes are supposed to be dark at any orientation under the polarized microscope if they were isotropic. The small difference of hole diameter between the PMMA capillary and mPOFs will not influence the alignment of the LC inside the air holes since the alignment of the LC is mainly determined by the surface tension of both LC and PMMA. This has also been demonstrated that the glass cylindrical cavities of 2um-6um infiltrated with liquid crystal present the same alignment [4].

4. Bandgap effect and thermal tunability of E7 infiltrated mPOFs

E7 is infiltrated into about 1cm of the 60cm long mPOF by using capillary forces for 5 minutes. After LC infiltration, the end of the mPOF filled with E7 is then butt-coupled to an SMF to study the bandgap effect and the thermal dependence of the spectral properties. A resistive hot stage (MC60+TH60, Linkam) is employed to heat up the part of the mPOF with LC in it. The transmission spectrum is recorded by the OSA with 1nm resolution, and normalized to that of the unfilled fiber as shown in Fig. 3. It is clearly seen that, by infiltrating the mPOF with E7, several bandgaps are formed in the transparency window of PMMA between 475nm to 800nm.
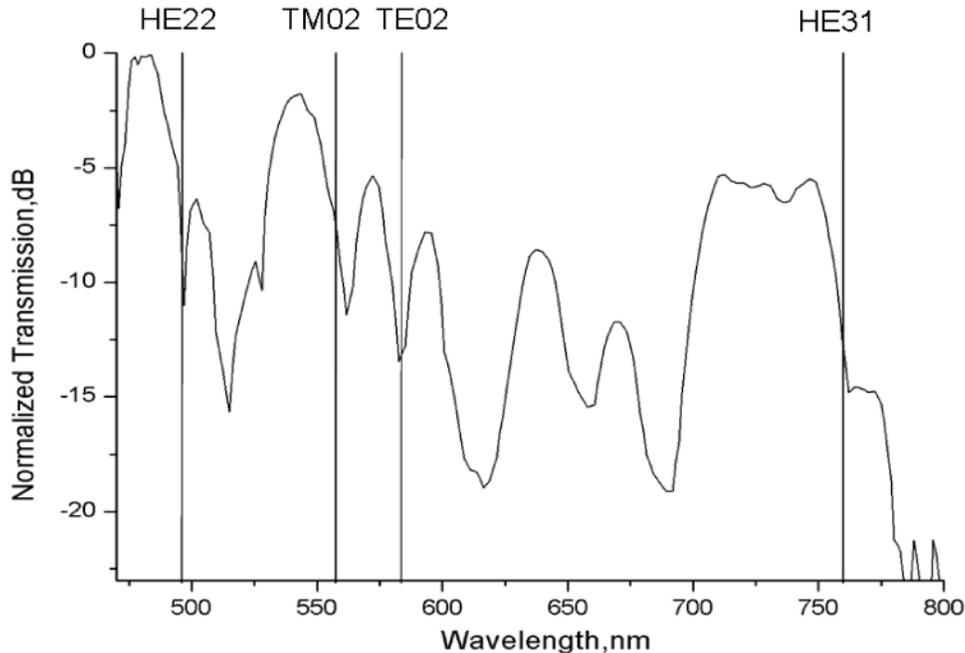

Fig. 3. Normalized transmission spectrum of the PMMA mPOF after infiltration with E7 for a length of 1cm. Modal cut-off wavelengths at 25°C are indicated with vertical lines.

To get a feeling of which bandgaps are situated where, we use the simple anti-resonant model [26]. According to this model the LC infiltrated holes may be approximated by isolated waveguides and the spectral features of the fiber can be estimated using a cut-off approach in the isotropic case, where minima in the transmission spectrum occur at the cut-off wavelengths of the guided modes supported by the LC filled holes. Since the E7 is an anisotropic material, the bands caused by the degenerate optical modes will inevitably split. Nevertheless, the birefringence and varying hole size of mPOF are not taken into account, because this would require a sophisticated numerical method, which was not the idea of using the simple model.

The simulations were performed by solving the wave equation using a freely available plane-wave tool [27], and both the dispersion of PMMA and E7 were considered. A supercell consisting of 8×8 elementary cells of the periodic cladding structure is used. The simulated cut-off wavelengths at T=25°C of the corresponding guided modes of the LC inclusions are marked with vertical lines in Fig. 3. As observed from Fig. 3, the optical mode of LP12 has been split into modes of HE22, TM02 and TE02 because of the anisotropy of E7. The numerically calculated cut-off wavelengths of HE22, TM02, TE02 and HE31 are in a good agreement with the experimental results.
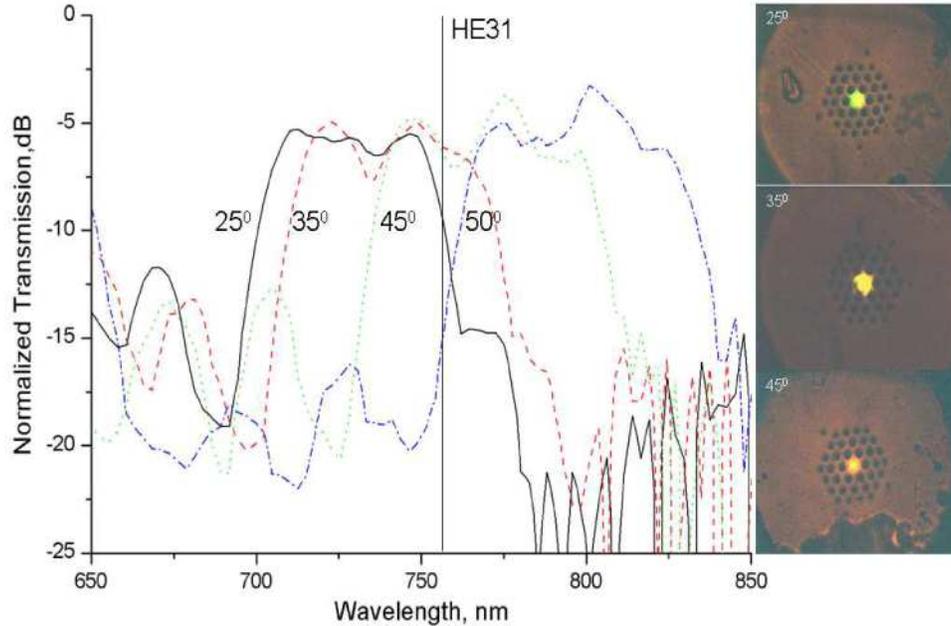

Fig. 4. Normalized transmission spectra of an E7 infiltrated mPOF for different temperatures from 25°C to 50°C. Insets show microscope images of the guided light of the E7 infiltrated mPOF at the indicated temperatures. The vertical line marks the calculated cut-off wavelength of the guided HE31 mode at T=25 °C.

The normalized transmission spectrum of the large bandgap in the wavelength range of 690nm-780nm is shown in Fig. 4 for different temperatures between 25°C and 50°C to demonstrate the thermal tunability. Using 3dB below the peak of the transmission to estimate the bandwidth of the bandgap, it is found that the bandgap has a bandwidth of about 65nm and a centre wavelength around 725nm at 25°C. As the temperature is increased, the bandwidth increases from 65nm to 85nm, and the centre of the bandgap shifts towards longer wavelengths. This red shift of the bandgap is due to the positive dn_o/dT of E7 [4], which results in an increasing ordinary refractive index (n_o) and thus an increasing index contrast between the background material PMMA and the LC as the temperature is increased towards the clearing temperature (T_c=58°C). With a fixed d/Λ, an increasing index contrast of the photonic bandgap fibers will increase the cut-off wavelengths of the modes guided inside the high-index inclusion, which will lead to the whole bandgap structure moving towards longer wavelengths [11,26].

Also shown in Fig. 4 are the microscope images of the guided light at different temperatures, from which we can see that the colour changes from red to green after infiltration, and then back towards red again when the temperature is increased. This again confirms that some wavelengths in the visible region are filtered out due to the E7 inducing bandgap effect and that the bandgaps are tuned by the temperature change.

5. Bandgap effect and thermal tunability of MDA-00-1444 infiltrated mPOFs

For comparison, about 1cm of MDA-00-1444 is infiltrated into an identical 60cm long mPOF for 10 minutes by applying capillary forces. The same setup is used to investigate the bandgap effect and thermal tunability. Figure 5 shows the normalized transmission spectra, which have high transmission in two bandgaps within the transparency window of PMMA: bandgap A centered at approximately 590 nm and bandgap B centered at approximately 780 nm at T=25°C.
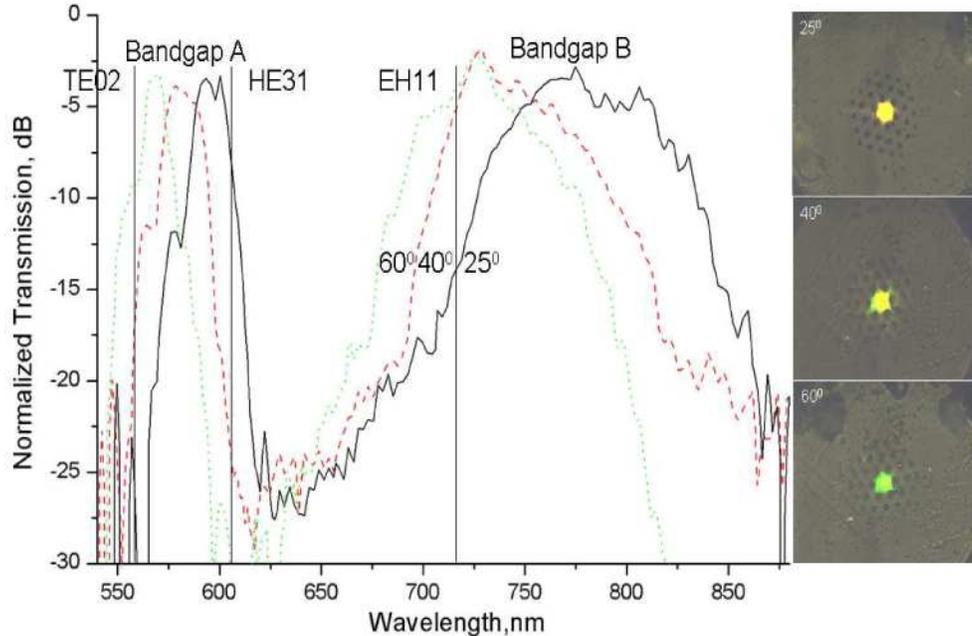

Fig. 5. Transmission spectra of the MDA-00-1444 infiltrated mPOF at temperatures 25°C, 40°C, and 60°C. All spectra are normalized to the transmission spectrum of the same unfilled mPOF. The microscope images of the inset show the colour variation of the guided light at different temperatures. The vertical lines mark the calculated cut-off wavelengths of the modes of the corresponding high-index inclusion at T=25 °C.

Figure 5 shows that, in contrast to what was observed for the E7 filled mPOF, the width of the bandgaps, especially that of bandgap B, are slightly reduced as the temperature of the MDA-00-1444 filled mPOF is increased from 25°C to 60°C, and at the same time, the centers of both bandgap A and bandgap B shift towards shorter wavelengths. The blue-shift of the bandgap centers is because of the negative dn_o/dT of the MDA-00-1444 [10], which means both the ordinary refractive index (n_o) of the LC and the index contrast between the background material and the LC decreases with increasing temperature.

The corresponding microscope images of the guided light at different temperatures, as shown in Fig. 5, verify a reverse colour change tendency compared with that of the E7 infiltrated mPOF, i.e., the colour of the guided mode varies from yellow to green with increasing temperature. We have calculated the modal cut-off wavelengths of the EH11, HE31, and TE02 modes of the MDA-00-1444 inclusion at T=25°C, which represent the stopbands in the anti-resonant model, and are marked in Fig. 5 with vertical lines.

6. Discussions and conclusions

In contrast to silica PCFs, mPOFs have a strongly oscillating loss in the near infrared range with regions of very high loss. In itself this creates bandgap like transmission windows, where the loss is so high that the transmission is effectively zero. The loss gaps, the temperature

sensitivity of polymers, and the birefringence of the mPOFs, are complicating factors that must be taken into account when studying the bandgaps of LC infiltrated mPOFs experimentally.

As observed in Figs. 4 and 5, the bandwidth of the bandgaps of LC infiltrated mPOFs are not constant and can be widened or narrowed by changing the temperature, in a quite similar way as for LC infiltrated silica photonic bandgap fibers. This implies that a different shift is experienced by the shorter and longer bandgap edge, i.e., the long-wavelength edge shifts more than the short wavelength edge. The difference in tuning sensitivity between the short- and the long-wavelength bandgap edge can be attributed to two reasons. Firstly, as described in the antiresonant model [26], the stopbands of bandgaps are represented by cutoff wavelengths of high-index inclusions, the overall increasing or decreasing of index of inclusions will cause both stopbands to shift toward longer wavelengths or shorter wavelengths with the same relative shift. Compared to the short-wavelength edge, this implies a longer absolute shift for the long-wavelength edge of bandgaps. Besides, the short-wavelength edge of the bandgap is defined by the higher order guiding modes of the high-index inclusion, while the long-wavelength edge of the same bandgap is defined by the lower order guiding mode. In general the lower order modes are confined better than the higher order modes, which implies that the lower order modes will experience more index change than the higher order modes and therefore a longer absolute shift should be observed for the long-wavelength edge of the bandgap. Secondly, since the two edges of the bandgaps are defined by different guided modes of the high-index inclusion, the different transversal and longitudinal distribution of the electric field of those modes will experience unequal index change due to the anisotropy of the LC, which results in different edge shifts with temperature [11,26].

We note that the transmission spectra of the MDA-00-1444 infiltrated mPOF display tilted bandgap edges and Gaussian shaped bands. These features are direct consequences of the material loss and the uneven distribution of hole size of our mPOF, combined with the birefringence of the LCs and the mPOFs.

The narrow bandgaps in the transmission spectrum of the E7 infiltrated mPOF, as shown in Fig. 3, are caused by the splitting of the effective indices of corresponding high order transversal electric modes (TE02) from the corresponding high order longitudinal modes (HE22, TM02) of the LC-infiltrated microchannels. The splitting is observed since the electric field of the transversal modes is mainly in the transversal direction, while the longitudinal modes have a part of the electric field in the longitudinal direction. The longitudinal modes therefore experience the extraordinary index of the LC and gaps in the effective indices are formed between the bands derived from those high order transversal and longitudinal cladding states [4]. In the current case, the birefringence of the mPOF and the non-uniformity of the size of the holes add more complexity to the bandgap analysis.

Estimated from 3dB below the peaks of the transmission spectra, as shown in Fig. 4 and Fig. 5, the thermal tuning sensitivities are measured at the long-wavelength edge of the bandgap to be about 4nm/°C and −1nm/°C for the E7 and the MDA-00-1444 infiltrated mPOFs, respectively. The difference in the thermal sensitivity is mainly caused by the difference in the temperature gradient and birefringence of the two kinds of LC [4,10]. If considering the thermal-optic coefficient of PMMA ($dn_o/dT = -1.1 \times 10^{-4}$/°C [12]) and the dn_o/dT of E7 and MDA-00-1444 at 656nm and 40°C, the roughly estimated thermal sensitivities of E7 and MDA-00-1444 infiltrated mPOFs are around 6nm/°C and −1.8nm/°C respectively, which are within the same order of our experimental observation. The slight difference is mainly due to the variation of the air hole size between the tested fibers and ideal calculation models, the small influence from the thermal-optic coefficient of extraordinary refractive index of liquid crystals, the material dispersion. Obviously a higher thermal tuning sensitivity would require a larger dn_o/dT, i.e., a higher birefringence and a lower clearing temperature [9,28].

For the LC infiltrated mPOF devices, the main origin of the insertion loss is the coupling loss between the index guiding modes and the bandgap guiding modes. However, the insertion loss is difficult to establish exactly due to Fabry–Pérot effects between the two end facets forming the butt coupling, which causes ripples in the transmission spectra. If we estimated the insertion loss from the peaks of the transmission spectra, we can find that the nominal insertion losses for E7 and MDA-00-1444 filled mPOF are about 5dB and 3dB respectively. These insertion losses are higher than those of LC infiltrated silica PCFs [3,4,6,9,10], which is due to the slightly worse mode confinement defined by the air hole ring number of the mPOF we used. Further optimization of the insertion losses can be achieved by using an mPOF with more rings of air holes.

Acknowledgements